Title
Design of Experiments Approach to Triboelectic Materials Testing

Author
Bekker, Logan

Publication Date
2023

Peer reviewed|Thesis/dissertation

Design of Experiments Approach to Triboelectric Materials Testing

By

LOGAN BEKKER

THESIS

Submitted in partial satisfaction of the requirements for the degree of

MASTER OF SCIENCE

in

Mechanical and Aerospace Engineering

in the

OFFICE OF GRADUATE STUDIES

of the

UNIVERSITY OF CALIFORNIA

DAVIS

Approved:

_____

Paul Erickson

_____

Andrew Pascall

_____

Cristina Davis

Committee in Charge

2023

Abstract

Interest in the applications of Triboelectric Nanogenerators (TENGs) has grown in the past decade as a means of effective energy harvesting in addition to its applications in powering low powered electronics and sensors especially in the area of Internet of Things (IoT). Majority of the research into TENGs focuses on maximizing the power output through different material combinations, material doping, topography manipulation, and design construction. However, unlike most energy sources common today such as solar, wind, piezoelectric and pyroelectric, the methods of measuring TENG output have not been established or agreed upon in the scientific community. This makes determining how a TENG will perform in a given design space difficult as the number of variables that can be adjusted are numerous.

A systematic approach to understanding the behavior of a TENG is with Design of Experiments (DOE). DOE can provide insight into the behavior of the TENG by adjusting parameters to determine what influences the output the most. The most common parameters that are altered in a TENG outside of material science are contact area, contact force and displacement distance of the two triboelectric materials.

The experimental results showed that the contact area and contact force affected output depending on the stage of contact separation that was measured (coming into contact vs separating), and that separation distance had almost no effect on voltage output.

Acknowledgments

I would like to express my appreciation and gratitude to my academic committee for their time and effort in helping me complete this thesis. Professor Erickson, you were always supportive and extremely helpful in guiding me on this winding path and I enjoyed that our discussions naturally detoured outside of just strictly academia and into more personal views of the world and interests. Dr. Andrew Pascall, you have been a pleasure to work with and get to know as a friend. You are someone I admire and look up to at Lawrence Livermore National Laboratory and I am glad you were interested in advising me on this thesis. Professor Cristina Davis, you were the first instructor I met when I began my graduate degree at UC Davis and were extremely accommodating to me as a distance learning student and I was thrilled to hear you would be able to join my thesis committee and lend your insight.

I want to thank Lawrence Livermore National Laboratory for giving me the opportunity to pursue this degree which otherwise I would not have been able to do. I am thankful to the vast number of supportive colleagues there who offered me a mountain of advice and recommendations to help me complete this work.

Most importantly, I owe and dedicate this work to my loving wife Diana Bekker. Words cannot describe the amount of support you have given me. I know this degree took longer than we agreed, but I am grateful for your patience and understanding. A lot happened to us while I completed this work, but I am so thankful you were by my side through all of it. I love you with all my heart.

This work was performed under the auspices of the United States Department of Energy by Lawrence Livermore National Laboratory (LLNL) under Contract DE-AC52-07NA2

IM Release number: LLNL-TH-845259

Table of Contents

List of Tables

List of Figures

Nomenclature

σ: Surface Charge Density

ε_0: Vacuum dielectric constant

3D: Three Dimension

AC: Alternating current

COTS: Commercial off the shelf

DOE: Design of Experiments

DC: Direct current

E_m: Maximized energy output

E_{em}: Maximized effective energy output

$FOM_{s,\ p\ m}$: Figure of Merit (Structural, Performance, Material)

IoT: Internet of Things

I_{sc}: Short Circuit Current

TECD: Triboelectric charge density

TENGs: Triboelectric Nanogenerators

V_{oc}: Open Circuit Voltage

1. Background

1.1. Introduction

Renewable energy has been a large talking point on the world stage in recent years. As the planet faces potential problems from the effects of climate change and fossil fuel use, renewable energy sources have been targeted to help mitigate the long term effects the planet is now beginning to experience.[1] Traditional renewable energy methods such as solar, wind, geothermal and hydrodynamic methods are commonly known and widely used throughout the world, however as technology has advanced, detailed avenues of renewable energy are being explored.[2]–[5]

One large field of renewable energy that has begun expanding is energy harvesters/scavengers that capitalize on the energy inefficiencies of many day-to-day systems. Energy harvesters/scavengers technically fall under the traditional renewable energy sources such as solar and wind, though commonly these refer to smaller devices that utilize the external energy of the environment. A classic example of such a harvester would be a device inside a shoe such as a piezoelectric that is able to charge a power supply as the user walks about.[6]–[8] The power that is generated from these devices is very low and has only recently seen application.

In addition to the expansion of the field of energy harvesting, the field of electronics has also continued to advance in reducing the size and energy requirements for components.[9], [10] The reduced energy requirements have opened the doors to alternative power methods outside of a traditional batteries or power supplies. The trend of reduced size and energy requirement is only continuing, and eventually extremely low powered sensors and electronics will be readily available.

The combination of advancements in electronic component power requirements and the expansion of energy scavengers and their output display an objective that is being accomplished from two sides. On one side you have the electronics field reducing the energy requirements of their components and devices and on the other side you have energy harvesters becoming more efficient and capable of powering the electronic components.[11], [12]

A promising energy harvester that has shown great promise is the triboelectric generator which uses triboelectricity to generate enough power for some of the available low-power electric components on the market.

1.2. What is triboelectricity

Triboelectricity is a subset of static electricity. Under static electricity, there are 3 primary methods to generate an electrical charge: triboelectricity, field induction and direct charging. Of the three, triboelectricity is the most common form of static electricity and what most people are familiar with. The triboelectric effect is the movement of electrons from the surface of one material to another through *electrostatic induction* caused by friction.[13], [14] In the classic example of rubbing a balloon against the hair on someone's head, the result of the persons hair standing on end is because electrons have been stripped from the strands of hair and now repel each other. This stripping of electrons caused by the friction of the balloon on the hair is the triboelectric effect. With triboelectricity, one material will strip electrons from the other based on how tribo-positive (Donator) or tribo-negative (Receiver) the materials are. When the two materials are separated the electrons that moved from donator to the receiver remain behind. As the distance is increased between the two materials an electric potential is created. When the two materials are brought back into contact with one another the voltage potential is reduced to zero.

In the balloon example when the balloon is pulled away the hair stands on end (voltage potential increase), when the balloon is brought back the hair is attracted to the balloon and can lay flat again (voltage potential reduced).

Figure 1: Child hair standing on end after being rubbed against balloon.[15]

Another example of triboelectricity is with commercial airplanes during flight. The simple action of the plane wing cutting through the air results in the air stripping electrons off the surface of the plane wing and creating a static charge. To mitigate this charge, airplanes have been fitted with static dischargers on the trailing edge of the wings to discharge the buildup into the atmosphere. The fact that a plane wing and body can generate an electric charge during flight is also why a specialized grounding cable is attached to the plane after landing and during refueling to prevent a static discharge that could result in a fire.

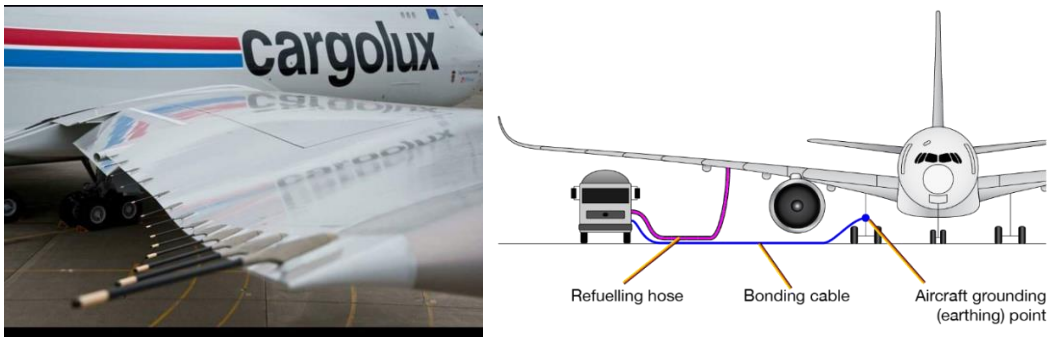

Figure 2: Electrostatic discharge prongs along trailing edge of aircraft. Aircraft must be discharged prior to refueling.[16]

1.3. Triboelectric series

The triboelectric phenomenon is based on the electron affinity of the materials selected and where they are ranked on the triboelectric series. Electron affinity is the degree to which a material will behave more as an electron donator or receiver as mentioned previously.[17], [18] The triboelectric series (Figure 3) is a qualitative list of commonly tested materials that ranks the materials by their electron affinity. When selecting a triboelectric pair, the greater the relative distance in rank of the two materials on the list (Top: tribo positive, Bottom: tribo negative) the greater the charge will be stripped during contact. It is still possible to create the triboelectric effect with similar materials that are close together on the list, however the number of electrons stripped will be low so the voltage potential created will be lower. Ideal materials for triboelectric generation are insulators as well as it has been observed that materials high in fluorine content, such as fluoropolymers, are excellent tribo-negative materials and should be paired with a high tribo-positive material for maximum voltage potential.[18], [19]

Recall the human hair and rubber balloon example. In the triboelectric series table below, fur/human hair is ranked relatively high as a tribo-positive material. Because human hair is tribo-positive, it will behave as a donator and is more likely to donate electrons to any material it comes into frictional contact with below it on the list. If human hair were paired with a pane of glass for example, it would behave as the tribo-negative material and strip electrons from the glass. Ranked below fur/human hair in Figure 3 is natural rubber which is in the tribo-negative ranking of this series. It can be expected that the rubber with act as the receiver in the tribo pair example.

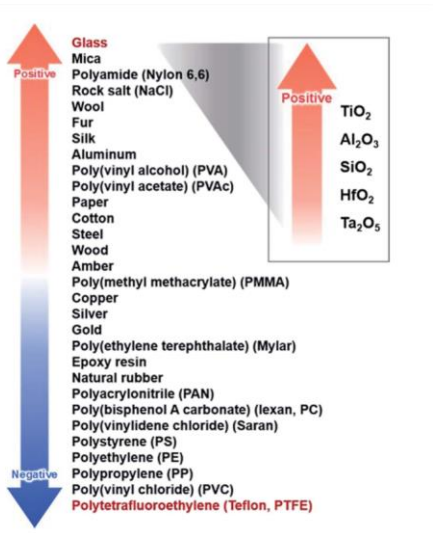

Figure 3: Qualitative triboelectric series of common materials.[20]

From the triboelectric series listed, we can assume that a combination of polytetrafluoroethylene (Teflon) paired with glass would have a greater triboelectric effect because of their relative ranking and placement on the extreme ends of the series.

While this specific triboelectric series is insightful, it is not exhaustive or all encompassing. There are many material sets actively being tested and investigated in the scientific community to achieve high triboelectric generation and output. The materials being explored involved doped material, surface topology manipulation, and internal structure modification.[21], [22] This shows that there is a vast space for material exploration and optimization in triboelectrics.

1.4. How is the triboelectric effect used to generate power?

As mentioned previously, when two tribo-opposite materials come into frictional contact an exchange of electrons occurs. When they are separated, an electric potential is generated in relation to one another. This potential arises from an imbalance of electrons between the

materials and the voltage potential remains until the two materials come into contact again. If the two materials are shorted with an electrically conductive wire however, this will also allow the electrons to equalize the electron imbalance. The movement of the electrons through the shorted wire creates current. In this system of two materials and a shorted wire, there is now a voltage potential (the two materials separated) and a way to drive current (the wire shorting the two materials). By connecting a load to the shorted wire between the two materials, the current generated by the triboelectric effect can power the load for as long as it takes for the electrons to move and equalize the imbalance. The fact that the potential is generated by the contact between the two surfaces resembles a "self-charging" capacitor that retains its charge until shorted through a circuit.[23], [24]

A common characteristic of static electricity is the voltage potential created is very large, however the current that can be generated is low. For example, lightning storms are essentially a massive triboelectric build up between the clouds and the earth, the voltage potential created before a lightning strike can be upwards to 300 million volts with the lightning strike driving up to 30,000 amps of current.[25] The same trend can be witnessed on a lab scale triboelectric device where a material pair capable of generating 5V during separation may have a current reading of 50 μA.

For these reasons, the ideal electrical loads to be powered via triboelectric devices needs to be small and low powered such as passive sensors. Triboelectric nanogenerators (TENGs) are a category of triboelectric devices that focus on energy harvesting that can provide enough power to low powered devices and sensors.[1] As technology has advanced and the energy requirement for electrical components have reduced, it has led to the viability of TENGs as a method for powering electrical loads.

1.5. How is the output measured?

The two most common metrics used when determining the output of a triboelectric pair is the *Open Circuit Voltage* (V_{oc}) and *Short-circuit Current* (I_{sc}). The voltage measurement of V_{oc} is an ideal case where the resistive load between two materials is infinite and prevents any current flow. Likewise, I_{sc} is the current measurement as if the resistive load were zero.

V_{oc} is typically measured through a multimeter or oscilloscope as they are typically configured with a 10Mohm or greater internal resistance which effectively acts as an open circuit and can measure the amount of potential between the two materials while limiting current flow as best as possible. I_{sc} is measured the same way as a normal current measurement through a multimeter or oscilloscope with a shunt resistor.

When a triboelectric material pair is tested using an oscilloscope or digital multimeter, regardless of the internal resistance, current will still flow and equalize the charge. In the figure below,

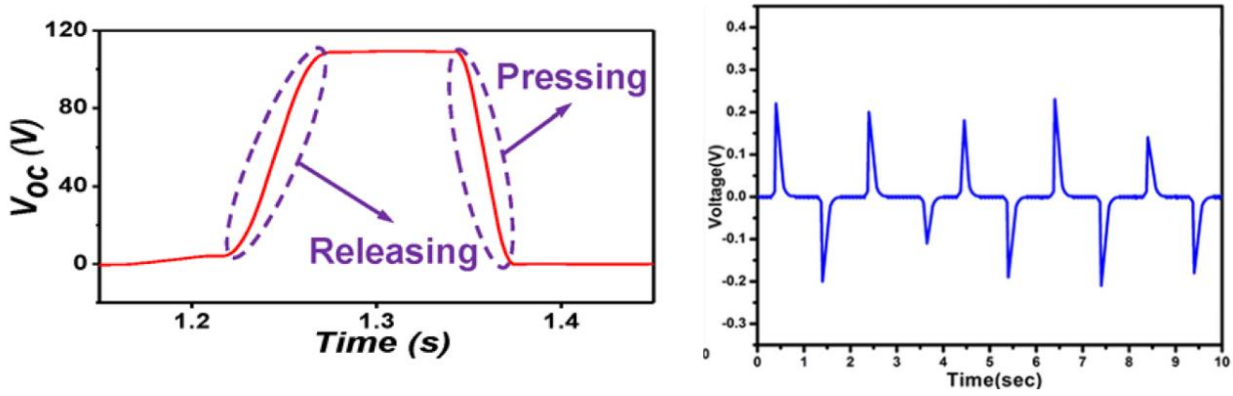

Figure 4 left, an ideal case of voltage measurement without any current flow is displayed. When measuring voltage through a physical device (oscilloscope or multimeter), electrons are still able to flow, and the voltage potential appears as a sharp spike that immediately decays to zero as the electron imbalance is corrected. The positive and negative spikes occur when the material pair are brought into contact and separated.

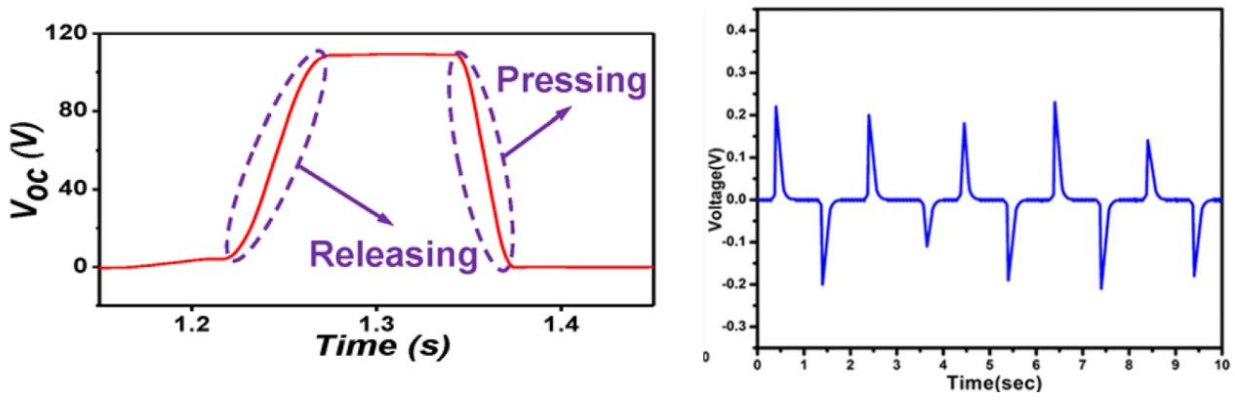

Figure 4: Left is theoretical voltage potential, assuming no electrons can flow between the two materials. Right is physically measured voltage potential through oscilloscope or DMM. Current is still able to flow through the system and equalize the electron imbalance.[1]

1.6. Contact modes of triboelectricity

There are four primary methods or modes for generating triboelectricity: contact separation mode, lateral sliding mode, single electrode mode, and freestanding triboelectric layer. All offer unique design considerations and advantages over each other.

1.6.1 Contact separation

Contact separation is the most common method of triboelectric generation. This method involves two planar tribo materials that come into flat contact and are separated via some method of displacement such as a spring.

The Figure 5 below illustrates how this method works. In the initial state of the two materials, they are at charge equilibrium. When they come into contact via a force, electrostatic induction occurs, and electrons are transferred to one of the materials. During the restorative force a

voltage potential is created and if there is no wire present the voltage potential remains indefinitely. When they are shorted the electrons return to their original material and drive current. After this point when the materials come into contact again (with a wire in place) the current immediately flows upon separation in one direction. When the materials are brought back together, current is also generated as the two materials have separate charges. This results in an alternating current as the electrons flow from material A to B upon release and from B to A when pressed together. AC current is a unique feature of triboelectric generation.

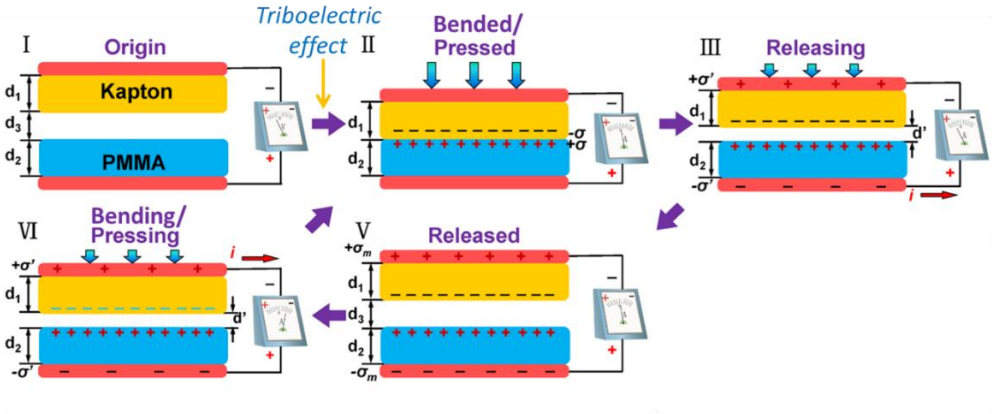

Figure 5 : Example diagram of contact separation mode of a triboelectric nanogenerator.[1], [26]

1.6.2 Single electrode

The single electrode is very similar to the traditional contact separation design. Whereas in the contact separation mode the movement of electrons is between the two material sets, in single electrode mode the movement of electrons come from a ground source. Additionally, in single electrode mode only one triboelectric material is necessary, the other can be a metallic electrode that is completely disconnected from the system.

Figure 6 below demonstrates the fundamental design of the single electrode. The contact between the disconnected electrode and the triboelectric material pulls electrons off the surface. The electrode below the triboelectric material is connected through a load to ground and the removal of electrons cause the movement of electrons from the ground source to pass through the load to equalize the potential on the surface of the electrode. When the disconnected electrode is brought back into contact with the equalized triboelectric material the excess electrons are “pushed” back through the load to ground.

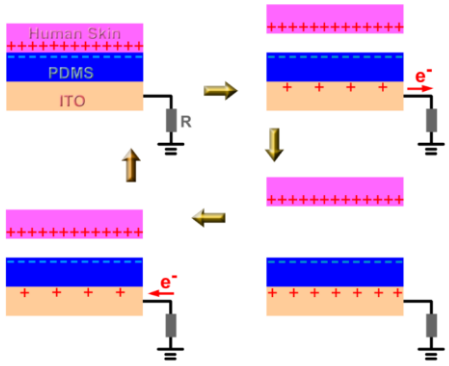

Figure 6: Single electrode mode triboelectric device wherein the load is in series with ground. Reproduced from Wang et al.[27]

1.6.3 Lateral sliding

Lateral sliding creates a planar imbalance of surface electrons between two materials. In this method the two tribo materials of the same contact area are in direct contact and shorted via a wire. In Figure 7 the top material is laterally shifted to one side so far that it leaves the edge of the bottom tribo material. This creates the electron imbalance as the electrostatic induction generated is applied only to the remaining top area still in contact with the bottom. When the electrons on the electrodes are examined, the tribo negative material (top material in this case) has retained electrons on its surface and the tribo positive material has lost electrons on the

surface of its electrode. The imbalance created this way drive current through the shorting wire and can be put through a load to power a device. This method will generate heat through friction and the amount of charge is limited in the amount of "overhang" that can be generated between the two materials.

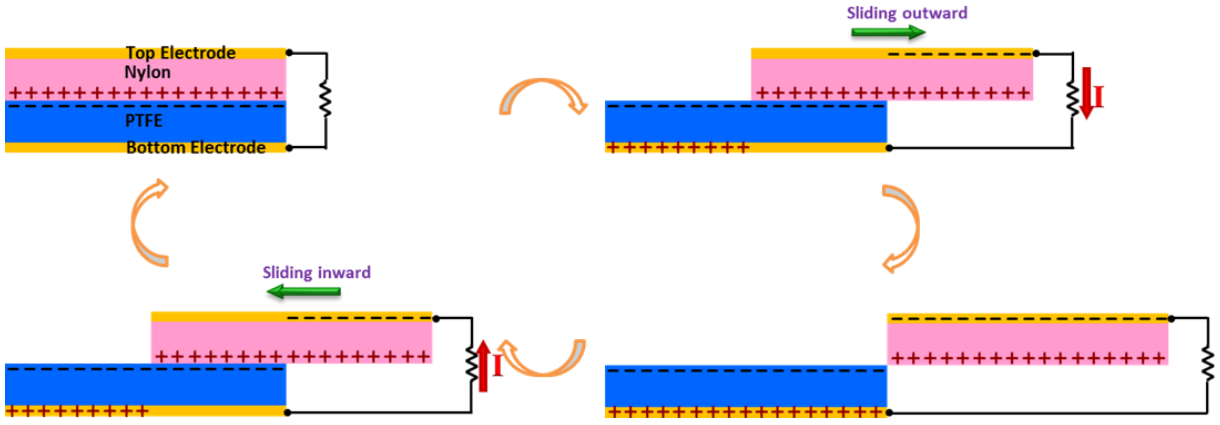

Figure 7: Diagram of lateral sliding triboelectric device. Reproduced from Wang et al.[28]

1.6.4 Freestanding triboelectric layer

Freestanding mode (Figure 8) involves having two of the same tribo materials connected through a wire with a load in series. The second tribo material is not directly connected to the system at all. This method has a combination of the lateral sliding method and the single electrode method, though instead of connecting to ground in the single electrode method, it is connected to another like tribo material.

To drive current in this mode, the freestanding material (that is not connected to the system) starts in contact with the first tribo material pad and is laterally moved much like the lateral sliding method. The electron imbalance is "pulled" to the second tribo material pad as the freestanding layer crosses a gap between to the two similar tribo material pads. The electron

imbalance created by the initial lateral sliding off the first tribo material creates an immediate imbalance on the second pad and drives the current through the wire to equalize the electron charge. Rapidly moving the freestanding layer between the two tribo pads creates a steady AC current output.

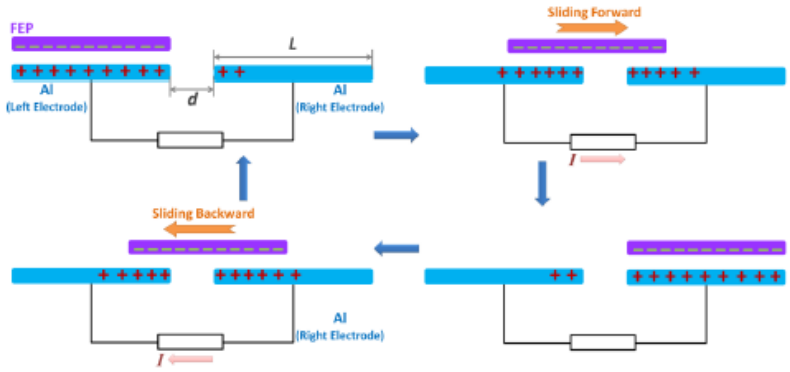

Figure 8: Lateral sliding move triboelectric device. Reproduces from Wang et al.[1]

1.7. Problem Statement

Triboelectricity is a phenomenon that has been well known for hundreds of years, however until recently with the large public interest into renewable energy has its research been pushed into new areas. There has been an explosion in research directions involving triboelectric output and design since the first large review article published by Zhong Lin Wang in 2016. Unfortunately, this field of study has no standardized reporting procedures which has led to ambiguity in published results. The main cause for this is that triboelectric output is influenced by many parameters such as contact area, surface topology, contact force, separation distance and triboelectric material selection which often times goes unreported.

1.8. Objective

The goal of this thesis is to provide an experimental test using a design of experiments methodology to determine the output of a given triboelectric material pair in contact separation mode. The design will cover of the primary variables in the triboelectric output: contact force, contact area, separation distance, and material selection.

1.9. Outline of thesis

This thesis will present a literature review of current literature practices and how authors take their data of triboelectric material pairs. Next this thesis will present an outline of an experimental approach to using a Design of Experiments (DOE) methodology which establishes a design space of different parameters to test within. DOE is common in many industries for measuring the effects of different independent variables of a system. Its aim is to be simple to follow and will provide accurate data that is useable and refined enough to be applied. A results and discussion section will follow to review the data taken with the method in the experimental approach section followed by a conclusion and recommendation section to conclude this thesis.

2. Literature Review

2.1. Introduction

The quantification of triboelectric output has begun to expand in the last decade. While other standards such as the ZT factor for thermoelectric, Carnot efficiency for pyroelectric nanogenerators and energy conversion efficiency for solar cells are well known, there is no standard for triboelectric output. Because the field of triboelectrics is relatively new, the output of material pair combinations is most generally examined as well as additional methods to increase output either through doping, topographical optimization, or creative design. This chapter will review proposed and currently used methods related to the focus of this thesis.

2.2. Review 1: Quantifying the triboelectric series[17]

In Zou et al., an attempt was made to create a standardization of the triboelectric series. To accomplish this, they tested dielectric polymers against liquid mercury with controlled environmental conditions. A metric was developed, Triboelectric Charge Density (TECD), by utilizing the contact separation mode inside of a faraday cage. In this case, the material pairs tested were a dielectric (polymer) to a conductor (metal) pair, similar to the single electrode design in Section 1.6.

The resulting work produced a list of over 50 materials and their calculated TECD, however Zou et al. did mention that the values produced are only qualitative estimation as contact separation triboelectrication can be achieved when two materials come into contact with one another, in this

case all the results were standardized against liquid mercury and the TECD would be different if the liquid mercury was changed out with a different material.

Liquid mercury was selected as the conductor pair because the authors believed the contact intimacy between the surfaces of the material would influence the output and the mercury would be capable of shaping to the surface of the dielectric material.

For their testing setup they had the dielectric material displace 75mm from the mercury surface as they determined that >10x the thickness of the dielectric material would create the largest voltage potential and chose that distance to measure the density of induced static charge at that point.

The following equations were used for the Dielectric-Conductor Contact separation mode:

For Voltage:

$$E_1 = \frac{\sigma_I(L,t)}{\varepsilon_1} \quad E_{air} = \frac{\sigma_I(L,t)-\sigma_c}{\varepsilon_0} \tag{1}$$

$$V = E_1 d_1 + E_{air} L \rightarrow \; V = \frac{\sigma_I(L,t)}{\varepsilon_1} d_1 + \frac{\sigma_I(L,t)-\sigma_c}{\varepsilon_0} L \tag{2}$$

For Current, V=0:

$$\sigma_I(L,t) = \frac{L\,\sigma_c}{\frac{d_1 \varepsilon_0}{\varepsilon_1} + L} \tag{3}$$

When $L >> (d_1\varepsilon_0/\varepsilon_1)$ the density of induced static charge ($\sigma_I(L,t)$) will equal the surface charge density (σ_c).

Zou et al. created a comprehensive catalogue of materials tested for the Triboelectric Charge Density (TECD); however, the authors did acknowledge that this list only shows half of the

solution to a TENG device and does not provide insight on how each material would perform with one another.

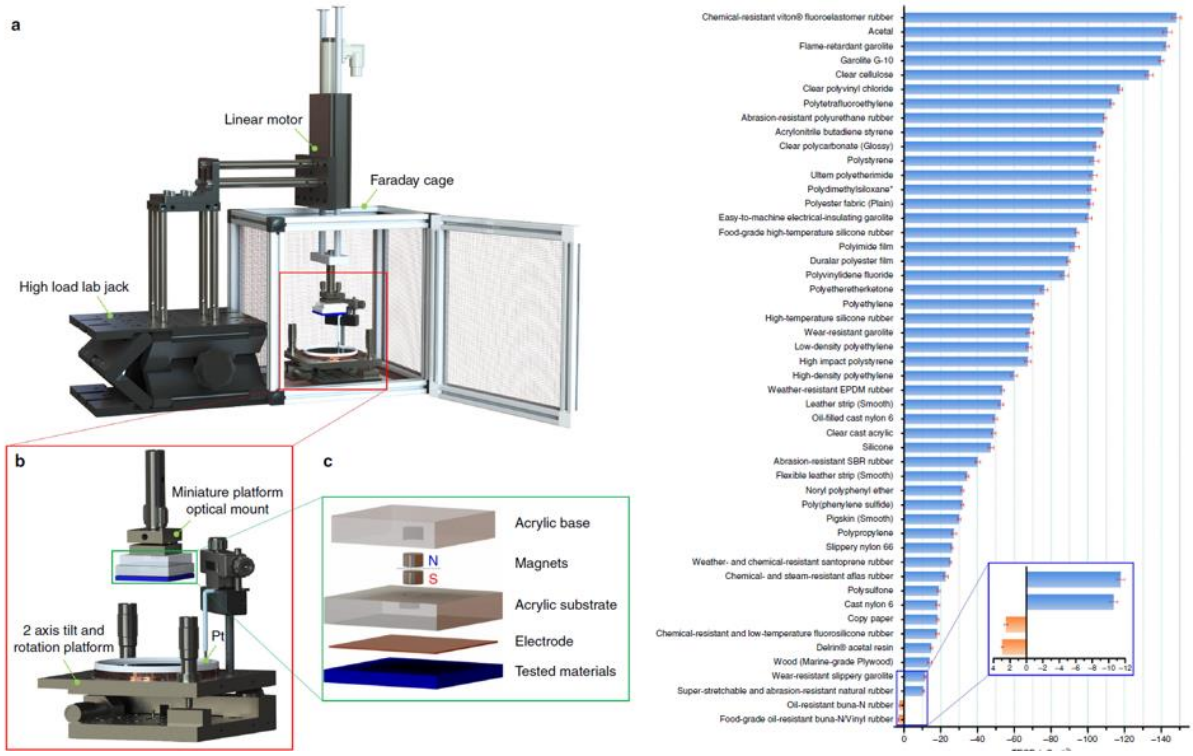

Figure 9: Left, experimental testing setup. Right, experimental ranking of each material from testing[17].

2.3. Review 2: Universal standardized method for output capability assessment of nanogenerators[23]

Xin et al.'s group aimed to create a universal standardization method that would be useful in determining the performance of a nanogenerator in practical applications. They believed that due to the high voltage potential created from triboelectric devices, it was possible that a voltage breakdown effect could occur as described in Paschen's Law.

Paschen's Law is the behavior of the voltage potential required to create an electric arc between two parallel plates at a given distance and pressure of a dielectric gas. Paschen's Law shows that as the distance between two plates at constant pressure is reduced, the voltage required to arc is reduced until a certain point where the voltage then increases.

Because of the voltage breakdown, Xin et al. believed that based on the theoretical V-Q plot created from a triboelectric device pair, that half of the chart is unreachable as voltage breakdown occurs.

To examine this behavior, the breakdown condition was measured by modeling the triboelectric system as a voltage source in series with a variable capacitor. The distance between the parallel plates were then varied in a feedback loop to determine the maximum displacement distance.

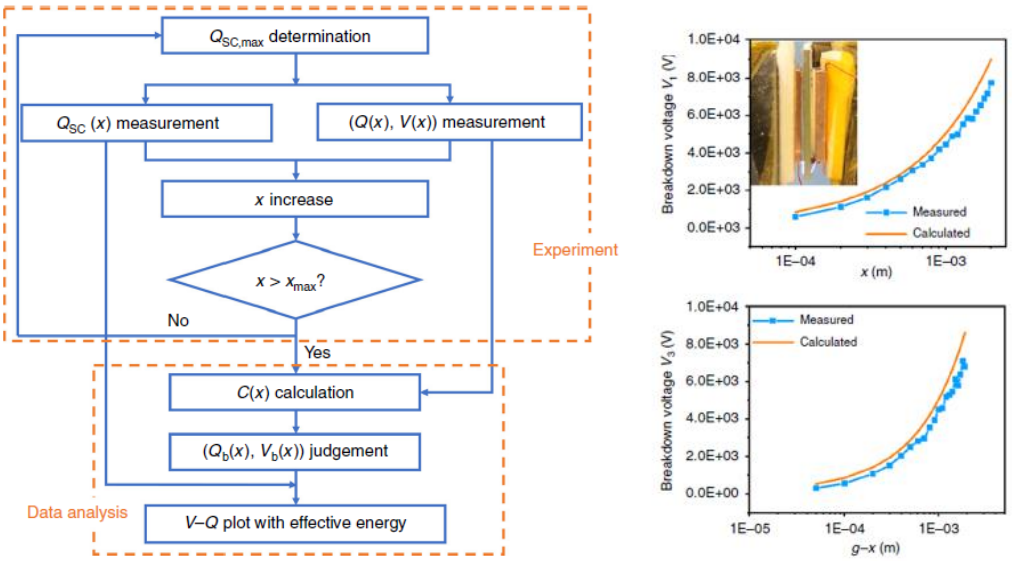

Figure 10: Left: Process flow used to determine the breakdown voltage of the triboelectric material set. Right: Measured average of voltage breakdown compared to calculated Paschen's Law theoretical values.

To accomplish this, Xin et al. constructed a closed loop testing station with samples in the contact separation configuration. The station would then tap the materials together and separate them. The system would then analyze the output and change the contact separation distance to maximize the output of the material pair. The goal of this was to achieve an experimental maximized effective energy output (E_{em}).

Using a previously defined figure of merit (FOM_s), they were able to redefine it accounting for the breakdown effect they witnessed during their tests:

Definition of Parameters	
FOM_s	Figure of Merit (Structural)
FOM_p	Figure of Merit (Performance)
FOM_m	Figure of Merit (Material)
ε_0	Vacuum dielectric constant
σ	Surface Charge Density
A	Triboelectrication area
X_{max}	Displacement max
E_m	Maximized energy output
E_{em}	Maximized effective energy output

$$FOM_s = \frac{2\varepsilon_0 * E_m}{\sigma^2 A x_{max}} \quad (4)$$

$$FOM_M = \sigma^2 \quad (5)$$

$$FOM_P = FOM_s * \sigma^2 \quad (6)$$

$$FOM_s = \frac{2\varepsilon_0 * E_{em}}{\sigma^2 A x_{max}} \quad (7)$$

$$FOM_p = FOM_s * \sigma^2 = 2\varepsilon_0 \frac{E_{em}}{A x_{max}} \quad (8)$$

The resulting equation created an updated Figure of Merit (from previous publications) that was consistent with their experiments and incorporated the behavior of Paschen's Law to determine the output capability of a Triboelectric Nanogenerator. This new FOM_P (performance) could be used to compare two different TENGs and determine which TENG will perform based on different mechanisms and structures. The authors used these equations to verify how a TENG performed based on its actuation configuration (contact separation vs freestanding layer) and concluded that the freestanding layer had a higher FOM than in contact separation.

2.4. Review 3: Design of Simulation experiments to predict triboelectric generator output using structural parameters[29]

Vasandani et al. created a simulated Design of Experiments (DOE) of two materials in contact separation mode using finite element analysis. The two materials they simulated were PET and polyimide. They created a 3 factorial experiment design and examined the parameters of contact area, displacement and material thickness in their model. The 3 factorial model was replicated 6 times for each experimental case for a total of 48 runs. One of the primary reasons this DOE was simulated rather than experimentally tested is due to how characterizing the surface charge density (σ) is difficult to quantify due to the many possible ways it can be changed as well as the type of equipment needed to measure it. They instead used a theoretical σ as a boundary condition.

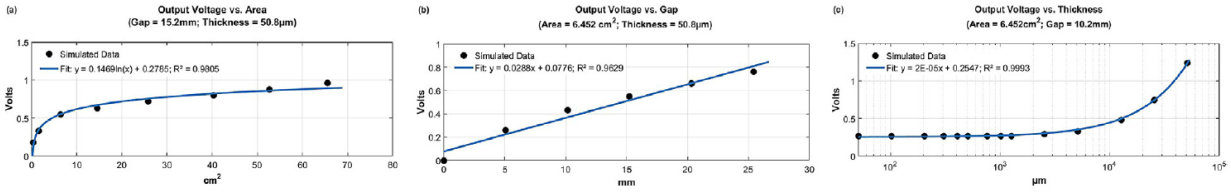

Fig. 3. Main effects of (a) area (b) gap, and (c) dielectric thickness on output voltage of triboelectric generator.

Figure 11: Main effects of (a) area (b) gap, and (c) dielectric thickness on output voltage of triboelectric generators

They created two experimental verification tests at the maximum and minimum parameters values for their design space (area: 6.45cm^2-25cm^2, distance: 4mm-12.5mm), however the material thickness was not changed. The thickness was not varied as their study of the main effects in Figure 11c show that the output based on thickness only comes into effect when the film thickness is greater than 500μm, instead they used 50.8μm films for their tests.

Their results of their simulation and experiments using an experimentally derived σ showed that x (separation distance) was the most influential structural parameter, followed by contact area. Film thickness had little to no influence on their system, though it was considered significant but an order of magnitude lower than area and separation distance.

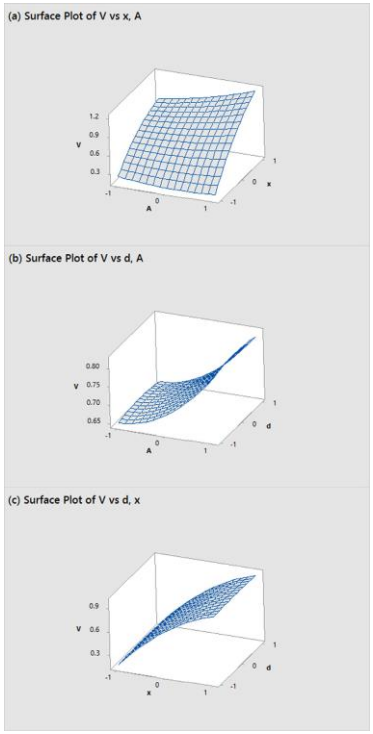

Figure 12: Surface plots of V vs (a) x, A, (b) d, A, and (c) d,x

3. Experimental Approach

3.1. Introduction

This chapter will discuss the method and equipment needed to test a triboelectric material pair in contact separation mode via a Design of Experiments (DOE) approach. DOE analysis allows for many parameters to be examined efficiently to determine the influence (main effects and interactions) on the outcome by reducing the number of experiments needed. Additionally, through randomization of the experiments it is possible to identify missed interactions during testing. The results are then examined for their significance to determine what parameters alone or combined have the greatest effect on the output.

Design of Experiment procedure:

- Determine independent input variables
    - Identify realistic upper and lower bounds of each variable
- Determine dependent output variables
- Determine possible sources of error/Shake-down or gauging
- Develop factorial chart where each input variable is tested at it max/min vs other input variables at their max/min
- Randomize tests and record outputs
- Calculate effects and interactions
- Determine statistical significance of results

The input variables for this DOE are the contact area (mm x mm), the contact force (N) and the separation distance (mm). A lower bound of 225mm^2 (15mm x 15mm) and upper bound of

2500mm^2 (50mm x 50mm) were chosen for the contact area. A lower bound of 1mm and upper bound of 35mm were chosen for the separation distance. A contact force of 1N and 10N were chosen for the lower and upper bounds respectively. The materials chosen for testing were cardstock paper and Teflon tape as these combinations are used often in literature and are present on triboelectric charts as triboelectric opposites.

Table 1 shows the matrix of testing configurations used for the DOE analysis. Each configuration is testing 3 times randomly.

Table 1: Testing configuration table

Configuration	**Area (mm^2)**	**Force (N)**	**Displacement (mm)**
A	225	1	1
B	2500	1	1
C	225	10	1
D	2500	10	1
E	225	1	35
F	2500	1	35
G	225	10	35
H	2500	10	35

3.2. Equipment used

Many of the components and equipment are considered commercial off the shelf (COTS) items with a few being fabricated through 3D printed additive manufacturing via a desktop 3D printer.

- Jenny Systems LX440 linear stage (44mm of travel)
- Jenny Science LINAX Servo Controller

- Keithley DMM 7510 7 ½ digit multimeter
- 80/20 Test Stand
- Sample holders (additively manufactured)
- Laptop

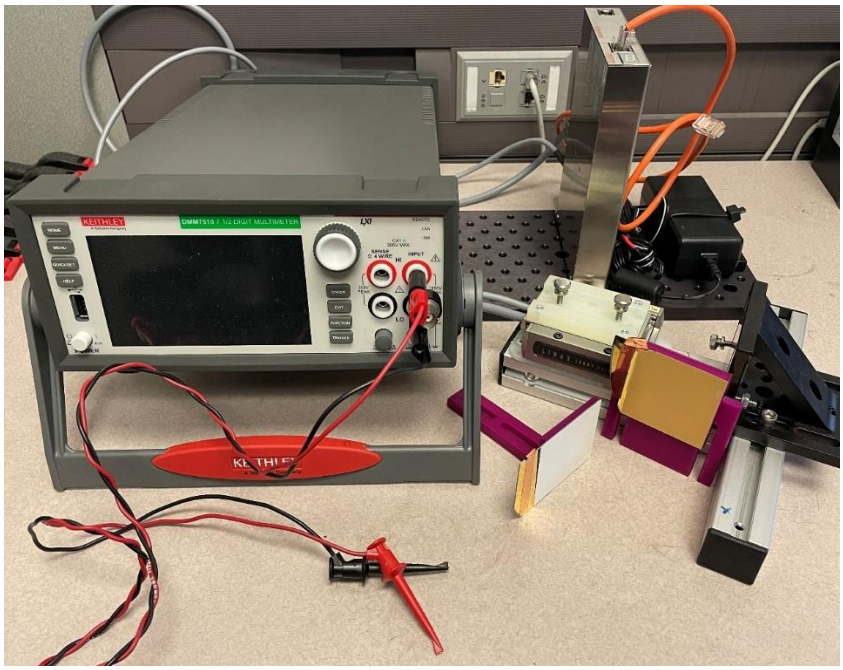

Figure 13: Testing components. Keithley DMM (left), Jenny Science servo controller (right, background) Jenny Science LX440 linear translation stage on 80/20 test stand (right, foreground), material test pads (purple parts)

3.3. Operation

When the testing protocol starts, the linear stage with mounted triboelectric material pair (Figure 14) will contact one another repeatedly at a given force and displacement as set by the user. Attached to each sample material is an electrical connection to a Keithley DMM7510 multimeter that measures the voltage output when the two materials come into contact. Following a

randomized testing pattern, each configuration is tested 3 times total across a total of 24 tests. The data collected from the test is saved under the run number in the randomized ordered. The peak values are recorded, and the average of each data set is used in the calculations table.

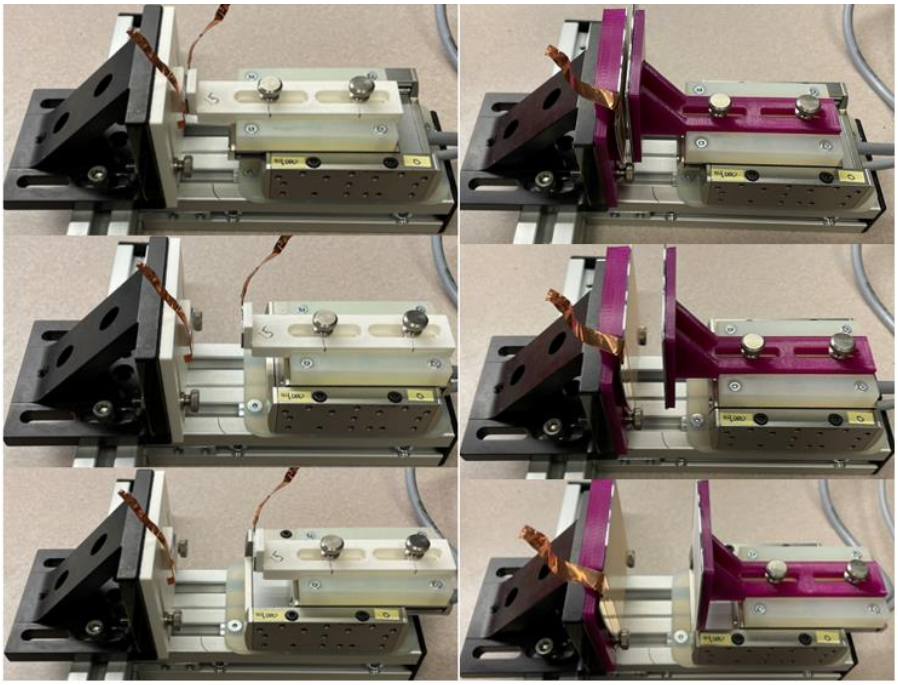

Figure 14: Testing setup of 225mm^2 and 2500mm^2 material plates on Jenny Science linear stage. Each photograph demonstrates the contact separation motion. Left column is the 225mm^2 sample test, right is 2500mm^2

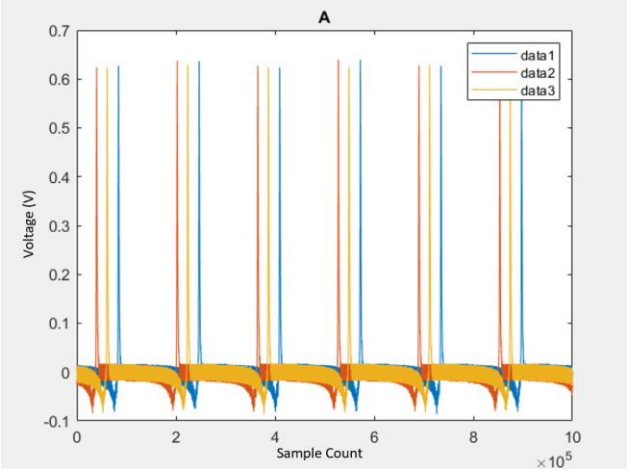

Figure 15: Example of the recorded voltage output from the contact of the two triboelectric materials pads (output is from configuration A).

3.4. Sample preparation

The materials used for the testing were adhered using conductive double sided carbon tape onto silicon wafer chips coated with gold measuring 55mm x 50mm, and 20mm x 15mm. A 5mm strip along the edge of each sample was added and to allow a proper electrical connection location on each sample. A strip of conducive copper tape was attached along the extra 5mm strip to act as an electrode to clip onto for testing resulting in each sample contact area being 50mm x 50mm and 15mm x 15mm. Between each randomized testing run, both surfaces were manually grounded with a wire connected to ground.

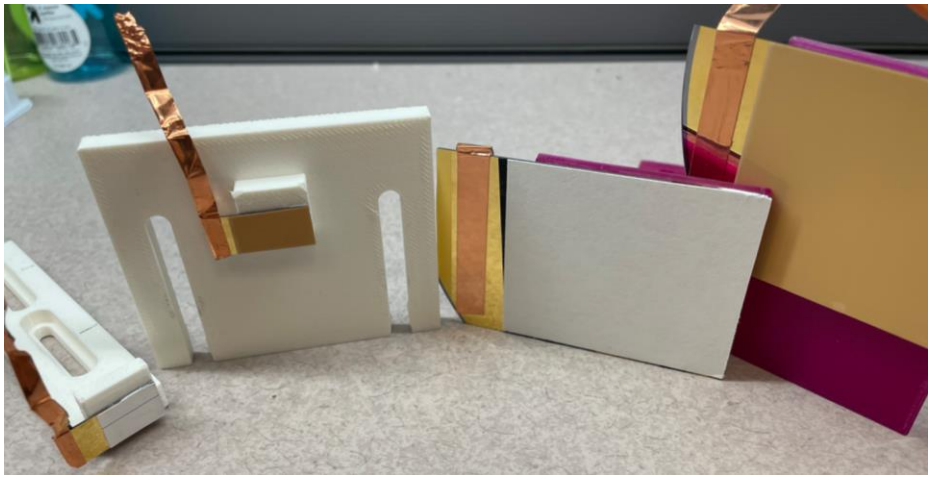

Figure 16: Triboelectric testing pads. Left 225mm^2 sample, right 2500mm^2 sample. Material is Teflon tape and cardstock

3.5. Experimental setup

Each sample was mounted onto a set of 3D printed polymer testing plates and held in place with double sided tape along the bottom of the sample. Once the samples had been mounted and in place, gator clips were attached to the copper tape electrodes and were connected to the Keithley DMM. Using the Jenny Science servo controller, the specified contact force and separation

distance was selected as per the randomized testing run configuration. The system is ready for testing.

3.6. Testing protocol

1) Reference the input variable parameters to be tested as per the randomized experimental order.
2) Enter the force and displacement values to be tested into the Jenny Science servo controller.
3) Attach the correct contact area sample plates to the Lxc linear stage and to the base stage with the knurled screws.
4) Start the initialization protocol. Allow the linear stage to move forward and back while the force sensor is calibrated.
5) Start the setup protocol. The linear stage will move forward until it contacts the base stage. It will move back to the entered displacement distance.
6) Ensure the electric connection clips are attached to the sample electrodes.
7) Ground each lead to remove any charge on the material sample.
8) Start the testing protocol. The Jenny Science motion stage will begin moving and start the data collection on the Keithley.
9) Once the buffer is full, save the data file to the removeable thumb drive with the test number as the filename.
10) Process the average peak value from the dataset and enter it into the corresponding configuration row of the DOE excel sheet.
11) Repeat steps for next configuration setup on the randomization test order.

4. Results and Discussion

4.1 Introduction

The initial results from testing revealed a limitation in the linear stage's ability to measure the forces applied during testing. In both cases in which the force applied was set to 1N or 10N, the force sensor would trip inaccurately. In all testing cases, more than 10N of force was applied to the sample set during testing regardless of the force sensors calibration. A result like this is common in the shake down process of a DOE and adjustments were made in the test setup approach.

The solution to this was to decouple the contact step and separation step during testing. To do this, for the contact step, the stage was set to a slow speed (0.015m/s) and a fast speed (1m/s), the displacement distances and contact areas were kept the same. This allowed for a better view of how the impact force would influence the output between both cases as the sensor lacked the sensitivity to accurately respond to the impact force.

For the separation step, the testing procedure began with the sample set separated by 1mm and would slowly move forward until the required force value was reached and then separate to a distance. This would ensure the force sensor would not trip due to sudden impact forces and would slowly reach the contact force expected. Two cases were examined where the sample set would separate at different speeds.

The data presented below examines how each parameter effects the design space for this experiment. The initial tables in each section display the measured voltage output for each configuration, the run order it was collected in, and the statistics of the three testing runs. The

table following the voltage output is the calculated main effects and interactions of the test data. This chart is created by assigning a +1 and -1 value to the max/min bounds of each parameter and analyzes how each main effect (contact area, force, displacement) and interaction (the products of two or more of the parameters) influences the output. Based on the signal to noise ratio, computed from the voltage averages and their +1/-1 voltages, a threshold is calculated to determine if the effect/interaction is significant to the regression equation. Coefficients are also calculated and presented in the table to create the regression equation for the predicted output given 3 parameters values that lie within the design space. Lastly, following the effects and interactions table is a bar chart displaying the comparative values of the coefficients of the regression equation. This plot is for a simplified and quick view as to which effects and interactions are significant in relation to one another. A blue line on the bar graph denotes the threshold for significance.

It is important to note that the results produced from this data apply only to this specific design space (combination of materials, parameters examined, method of examination) and can lend insight on how parameters interact with one another but are not a definitive solution to all triboelectric testing behaviors.

4.2 Testing Results

4.2.1 Fast Contact Results

The results of the Fast Contact test, where the carriage moved forward at a rate of 1m/s are listed in Table 2. From the data, configuration 7 produced the highest voltage output (1.215V) with configuration 3 slightly lower (1.083V). The only difference between these two configurations

were the displacement distance between the two material surfaces. Configurations C and G have the smaller contact area (225mm^2) and the highest force (10N) of the testing configurations.

Conversely, configurations B and F were the lowest performers (0.265V and 0.276V respectively) from the data with the largest contact area (2500mm^2). Their averaged voltage output only differed by 0.011V despite having 1mm and 35mm separation distances.

An initial look at the results of the Fast Contact data set implies there an inversely proportional voltage output between the contact areas. Despite the slight voltage differences between 1mm and 35mm separation, the output voltages remain relatively the same. Between each configuration in Table 2, the variance of the average voltage values is very low signifying the dispersion of the data is very close together and accurate.

Table 2: Fast Contact Results

Configuration	Actual Run Order	C. Area	Force	Displacement	Yrep1	Yrep2	Yrep3	Average (Y)	StDev (Y)	Variance (Y)
A	22,11,16	225	1	1	0.631	0.632	0.624	0.629	0.004	1.8E-05
B	13,21,23	2500	1	1	0.273	0.264	0.259	0.265	0.007	5E-05
C	**2,4,15**	**225**	**10**	**1**	**1.096**	**1.079**	**1.076**	**1.083**	**0.011**	**0.00012**
D	10,14,7	2500	10	1	0.525	0.526	0.526	0.526	0.000	2.3E-07
E	6,3,12	225	1	35	0.651	0.640	0.645	0.645	0.005	2.7E-05
F	24,17,18	2500	1	35	0.267	0.281	0.278	0.276	0.007	5.3E-05
G	**9,1,20**	**225**	**10**	**35**	**1.229**	**1.213**	**1.205**	**1.215**	**0.012**	**0.00015**
H	8,19,5	2500	10	35	0.593	0.599	0.591	0.594	0.004	1.9E-05

Table 3 shows the calculated effects (directly from parameters) and interactions (the combination of products of the parameters). The effects in bold represent statistically significant effects on the output of the test system. The coefficients in bold can be used to create a regressive equation

that can be used to back calculate an output when given parameters within the design space to test.

The effects row shows that in this case all effects and interactions are considered statistically significant however, Figure 17 presents a bar graph of the relative contribution to the output. Figure 17 shows that the greatest influence in voltage output for this design space is contact area (E_1) and force (E_2). There is a horizontal blue line toward the bottom of Figure 17 which sits below all values in the bar chart which identifies the cutoff point of significance. While all effects and interactions as calculated are significant it is also representative of the accuracy of the data analyzed. It shows that while the significance of effects is minor for example, their contribution to accuracy of the regressive equation is beneficial to produce a high R^2-value equation (for this dataset, the R^2-value is 99.96%).

An important effect to notice is the contact area (E_1) coefficient is negative. This means that as the contact area increases, it negatively impacts voltage output. Recalling the earlier observation about Table 2 regarding inverse proportionality of voltage output, the negative coefficient verifies its behavior.

Table 4 offers better clarity of this effect of the negative contact area effect. When converting the contact area and force applied to pressure for configurations with max/min contact area and max/min forces the trend is easier to see that pressure is a driving factor in voltage output in this testing case. The configuration with the smallest contact area ($225mm^2$) and highest force (10N) produces a pressure of 44.4kPa and 1.096V and 1.215V while at the other end of the test design space, the largest contact area ($2500mm^2$) and lowest force (1N) produced a pressure of 400Pa and a voltage of 0.276V and 0.265V.

The last notable observation from this dataset is how little influence the displacement of the two contact pads has on voltage output.

Table 4 included the voltage output from both the 1mm displacement and 35mm displacement test and still the compared voltages between min and maximum displacement vary only slightly.

Table 3: Calculation of Effects and Coefficients for Average (Y), Fast Contact

	Constant	E_1	E_2	E_3	I_{12}	I_{13}	I_{23}	I_{123}
Avg(Avg(Y)) @ +1:		0.4153	0.8547	0.6826	0.59855	0.64553	0.67603	0.64712
Avg(Avg(Y)) @ -1:		0.8933	0.4538	0.6259	0.70998	0.663	0.63249	0.6614
Effect (Delta):		**-0.478**	**0.4009**	**0.0568**	**-0.1114**	**-0.0175**	**0.04353**	**-0.0143**
Coefficient (Delta/2):	0.65426137	-0.239	0.2005	0.0284	-0.0557	-0.0087	0.02177	-0.0071
SE Coefficient:	0.00149968	0.0015	0.0015	0.0015	0.0015	0.0015	0.0015	0.0015
T-Value	436.266204	-159.4	133.67	18.926	-37.151	-5.8255	14.5145	-4.7619
P-Value	4.8951E-34	5E-27	8E-26	2E-12	5.9E-17	2.6E-05	1.3E-10	0.00021

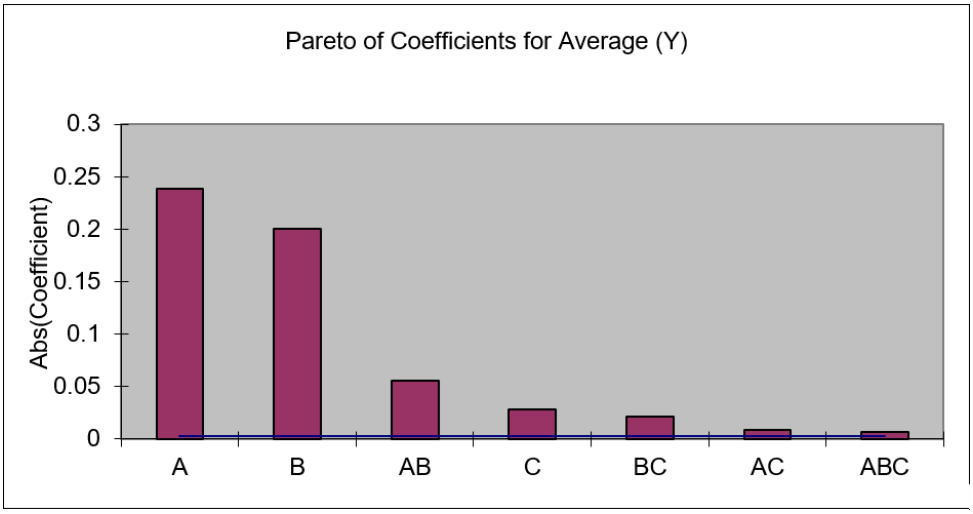

Figure 17: Effects of parameters for Fast Contact test. Bar graphs represent relative effect on testing output. All coefficients are statistically significant.

Table 4: Pressure Comparison, Fast Contact

Contact Area (mm^2)	*Force (N)*	*Pressure (Pa)*	*Output Voltage (V)*	*Testing Configuration*
225	1	4444.44	0.629	A
			0.645	D
225	10	44444.44	1.096	C
			1.215	G
2500	1	400	0.276	F
			0.265	B
2500	10	4000	0.526	D
			0.594	H

4.2.2 Slow Contact Results

The setup for the Slow Contact data had the linear stage speed set to 0.1m/s, like the Fast Contact dataset. Table 5 shows a similar trend as was observed in the Fast Contact data set, configuration C and G produced the highest voltage output at 0.766V and 0.751V respectively. Additionally, configuration B and F also produced the lowest (0.151V and 0.153), attributing to the lower amount of pressure as discussed in the Fast Contact results section. Variance for all data values remains low indicating accuracy of the data however Table 6 shows that not all effects and interactions are significant like in the Fast Contact dataset.

Table 5: Slow Contact Results

Configuration	Actual Run Order	C. Area	Force	Displacement	Yrep1	Yrep2	Yrep3	Average (Y)	StDev (Y)	Variance (Y)
A	22,11,16	225	1	1	0.3340	0.3344	0.3368	0.3351	0.0015	2.4E-06
B	13,21,23	2500	1	1	0.1507	0.1537	0.1490	0.1511	0.0024	5.6E-06
C	**2,4,15**	**225**	**10**	**1**	**0.7765**	**0.7742**	**0.7480**	**0.7662**	**0.0158**	**0.00025**
D	10,14,7	2500	10	1	0.3720	0.3676	0.3686	0.3694	0.0023	5.3E-06
E	6,3,12	225	1	35	0.3503	0.3433	0.3337	0.3424	0.0083	6.9E-05
F	24,17,18	2500	1	35	0.1550	0.1508	0.1560	0.1539	0.0028	7.8E-06
G	**9,1,20**	**225**	**10**	**35**	**0.7673**	**0.7463**	**0.7400**	**0.7512**	**0.0143**	**0.0002**
H	8,19,5	2500	10	35	0.3790	0.3727	0.3627	0.3714	0.0082	6.8E-05

Table 6: Calculation of Effects and Coefficients for Average (Y), Slow Contact

	Constant	E_1	E_2	E_3	I_{12}	I_{13}	I_{13}	I_{123}
Avg(Avg(Y)) @ +1:		0.2615	0.5646	0.4047	0.35458	0.40667	0.40221	0.40779
Avg(Avg(Y)) @ -1:		0.5487	0.2456	0.4055	0.45562	0.40353	0.40798	0.4024
Effect (Delta):		**-0.287**	**0.3189**	-7E-04	**-0.101**	0.00313	-0.0058	0.00539
Coefficient (Delta/2):	**0.40509792**	**-0.144**	**0.1595**	-4E-04	**-0.0505**	0.00157	-0.0029	0.00269
SE Coefficient:	0.00178719	0.0018	0.0018	0.0018	0.00179	0.00179	0.00179	0.00179
T-Value	226.667107	-80.37	89.232	-0.199	-28.268	0.877	-1.6137	1.50725
P-Value	**1.7331E-29**	**3E-22**	**5E-23**	0.8451	**4.4E-15**	0.39347	0.12613	0.15124

Table 6 also shows the same trend where the coefficient for the contact area (E_1) is negative (-0.287) which is to be expected as the testing set up is identical to the Fast Contact setup but with a different speed except the magnitude is different. Figure 18 show the comparison of the effects and how the separation distances and all interactions with it are below the blue cutoff line of

significance. The regression equation for this data set will only include the contact area, force and the interaction of contact area multiplied by the force.

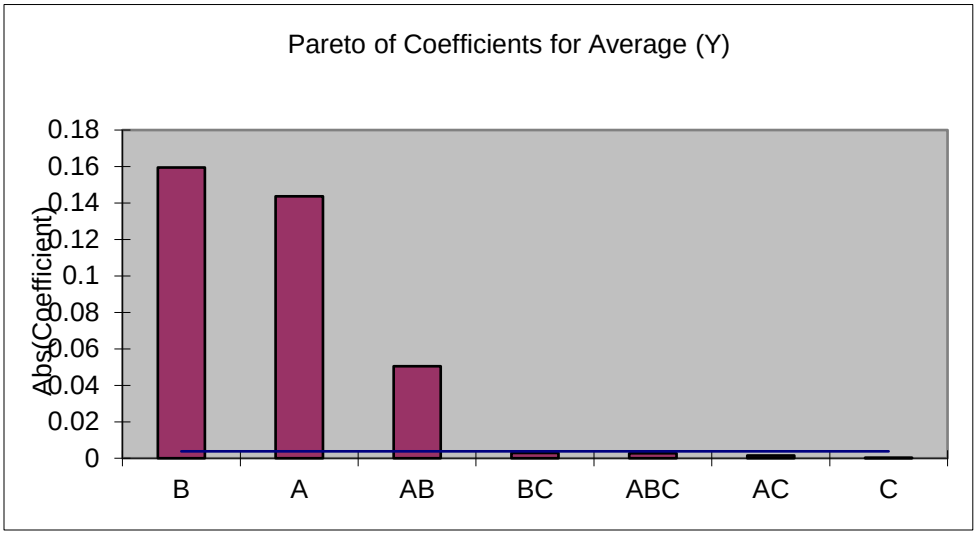

Figure 18: Effects of parameters for Slow Contact test. Bar graphs represent relative effect on testing output. Horizontal blue line signifies cut off limit for statistical significance.

4.2.3 Fast Separation Results

The Fast Separation setup involved having the contact plates separated by 1mm and would slowly advance to contact the two material pads together until the configuration force was reached and would then displace the contact pad on the linear stage away at different speeds. In this setup the displacement speed was set to 0.2m/s and acceleration of 0.01m/s^2. The slow approach to contact and slow loading of force of the contact pads enabled an accurate response from the force sensor in the linear stage.

Table 7 summarizes the data and shows that configurations D and H produced the highest output voltage (0.268V and 0.302V respectively). The lowest output configurations were C and A at 0.027V and 0.031V, however all configuration that had 225mm^2 contact area performed between

27-36mV output whereas the larger contact area configurations produced voltages in the 130-300mV range, almost an order of magnitude higher. At a glance, this difference could imply the significance of the contact area in this testing setup.

Table 7: Fast Separation Results

Configuration	Actual Run Order	C. Area	Force	Displacement	Yrep1	Yrep2	Yrep3	Average (Y)	StDev (Y)	Variance (Y)
A	22,11,16	225	1	1	0.0300	0.0312	0.0310	0.0307	0.0006	4.1E-07
B	13,21,23	2500	1	1	0.1395	0.1364	0.1360	0.1373	0.0019	3.6E-06
C	2,4,15	225	10	1	0.0280	0.0264	0.0279	0.0274	0.0009	7.4E-07
D	**10,14,7**	**2500**	**10**	**1**	**0.2734**	**0.2662**	**0.2653**	**0.2683**	**0.0045**	**2E-05**
E	6,3,12	225	1	35	0.0361	0.0360	0.0365	0.0362	0.0003	6.8E-08
F	24,17,18	2500	1	35	0.1412	0.1396	0.1318	0.1375	0.0051	2.6E-05
G	9,1,20	225	10	35	0.0372	0.0373	0.0358	0.0367	0.0009	7.4E-07
H	**8,19,5**	**2500**	**10**	**35**	**0.3112**	**0.3102**	**0.2873**	**0.3029**	**0.0135**	**0.00018**

In Table 8 all effects and interactions are considered significant, which lends itself to the small variance of the data in Table 7. Additionally, in the separation stage on the contact-separation mode, the contact area (E_1) effect is positive unlike during the contact stage previously discussed. Figure 19 compares the significance of each effect, where contact area is most significant at almost twice that of force (E_2) and the interaction of contact area and force (I_{12}). Table 8 shows that all interactions are significant, however when compared with the bar graph in Figure 19 it can be seen how little influence the separation distance has on the regression equation and raw output voltage values.

Table 8: Calculation of Effects and Coefficients for Average (Y), Fast Separation

	Constant	E_1	E_2	E_3	I_{12}	I_{13}	I_{13}	I_{123}
Avg(Avg(Y)) @ +1:		0.2115	0.1588	0.1283	0.15953	0.12464	0.12692	0.12596
Avg(Avg(Y)) @ -1:		0.0328	0.0854	0.1159	0.08475	0.11964	0.11737	0.11833
Effect (Delta):		**0.1787**	**0.0734**	**0.0124**	**0.07478**	**0.005**	**0.00955**	**0.00763**
Coefficient (Delta/2):	**0.12214191**	**0.0894**	**0.0367**	**0.0062**	**0.03739**	**0.0025**	**0.00477**	**0.00382**
SE Coefficient:	0.00110529	0.0011	0.0011	0.0011	0.00111	0.00111	0.00111	0.00111
T-Value	110.506626	80.85	33.204	5.6052	33.8298	2.26174	4.31997	3.45325
P-Value	**1.6887E-24**	**2E-22**	**3E-16**	**4E-05**	**2.6E-16**	**0.03799**	**0.00053**	**0.00327**

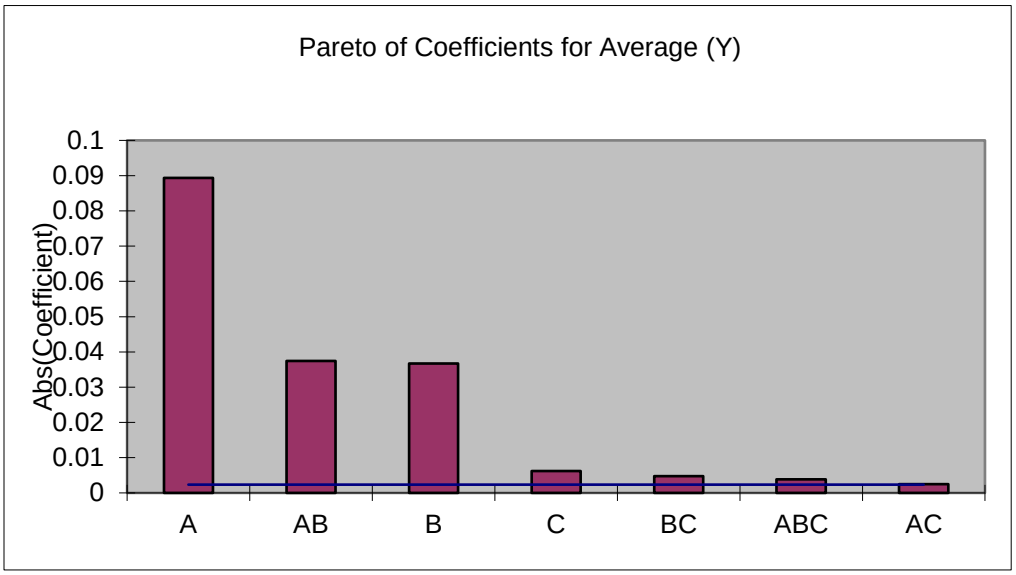

Figure 19: Effects of parameters for Fast Separation test. Bar graphs represent relative effect on testing output. Horizontal blue line signifies cut off limit for statistical significance

4.2.4 Slow Separation Results

For the slow separation setup, the linear stage displacement speed was set to 0.01m/s with an acceleration of 0.001m/s^2 compared to the fast separation setup with 0.01m/s velocity and 0.01m/s^2 acceleration.

Like the Fast Separation results, Table 9 shows configuration D and H produced the highest voltage output (0.419V and 0.418V respectively) which have both the largest contact area and highest force. Configurations B and F have similar voltages (0.314V and 0.223V respectively) to configurations D and H while having the same contact area but the lowest applied force. This initial glimpse of the data suggests that the contact area has a greater effect on output compared to force as even the lower force configurations with the same contact area produced less voltage. All configurations with the smaller contact area produce very low voltage regardless of force applied by almost an order of magnitude compared to the larger contact area configurations. The distance of displacement of the samples appears to have little noticeable effect to the voltage output in all configurations tested.

Table 9: Slow Separation Results

Configuration	Actual Run Order	C. Area	Force	Displacement	Yrep1	Yrep2	Yrep3	Average (Y)	StDev (Y)	Variance (Y)
A	22,11,16	225	1	1	0.0219	0.0223	0.0229	0.0224	0.0005	2.6E-07
B	13,21,23	2500	1	1	0.3750	0.3560	0.2123	0.3144	0.0889	0.00791
C	2,4,15	225	10	1	0.0264	0.0268	0.0286	0.0273	0.0012	1.3E-06
D	**10,14,7**	**2500**	**10**	**1**	**0.4338**	**0.4140**	**0.4114**	**0.4197**	**0.0123**	**0.00015**
E	6,3,12	225	1	35	0.0355	0.0357	0.0372	0.0361	0.0009	8.6E-07
F	24,17,18	2500	1	35	0.2272	0.2237	0.2201	0.2236	0.0036	1.3E-05
G	9,1,20	225	10	35	0.0257	0.0262	0.0262	0.0261	0.0003	7.9E-08
H	**8,19,5**	**2500**	**10**	**35**	**0.4237**	**0.4283**	**0.4020**	**0.4180**	**0.0141**	**0.0002**

Compared to the Effects and Coefficients table for the Fast Separation test, Table 10 shows there is no significance for the main effect or interactions with displacement distance. This result is similar to the Fast and Slow Contact Data in that all effects and interactions were significant for the Fast case but all interactions with displacement dropped off for the Slow case.

When looking at the visual comparison of the effects in Figure 20, contact area (E_1) is considerably higher (almost 4 times) than force (E_2) or the interaction between force and contact area (I_{12}). This trend was seen in the raw data in Table 9 where the configurations with the largest contact area produced the highest voltage.

The main effect of force (E_2) and interaction of contact area and force (I_{12}) are almost identical in this testing setup at 0.073 and 0.076 respectively. This main effect and interaction are also very close to the same coefficients in the Fast Separation Effects table (0.73 and 0.74).

Table 10: Calculation of Effects and Coefficients for Average (Y), Slow Separation

	Constant	E_1	E_2	E_3	I_{12}	I_{13}	I_{13}	I_{123}
Avg(Avg(Y)) @ +1:		0.344	0.2228	0.176	0.22405	0.17282	0.19522	0.19896
Avg(Avg(Y)) @ -1:		0.0279	0.1491	0.196	0.14786	0.19908	0.17668	0.17294
Effect (Delta):		**0.316**	**0.0736**	-0.02	**0.07619**	-0.0263	0.01853	0.02601
Coefficient (Delta/2):	**0.18595186**	**0.158**	**0.0368**	-0.01	**0.0381**	-0.0131	0.00927	0.01301
SE Coefficient:	0.00656433	0.0066	0.0066	0.0066	0.00656	0.00656	0.00656	0.00656
T-Value	28.3276325	24.071	5.6096	-1.524	5.80339	-1.9999	1.4117	1.98148
P-Value	**4.2258E-15**	**5E-14**	**4E-05**	0.1471	**2.7E-05**	0.06278	0.17719	0.06499

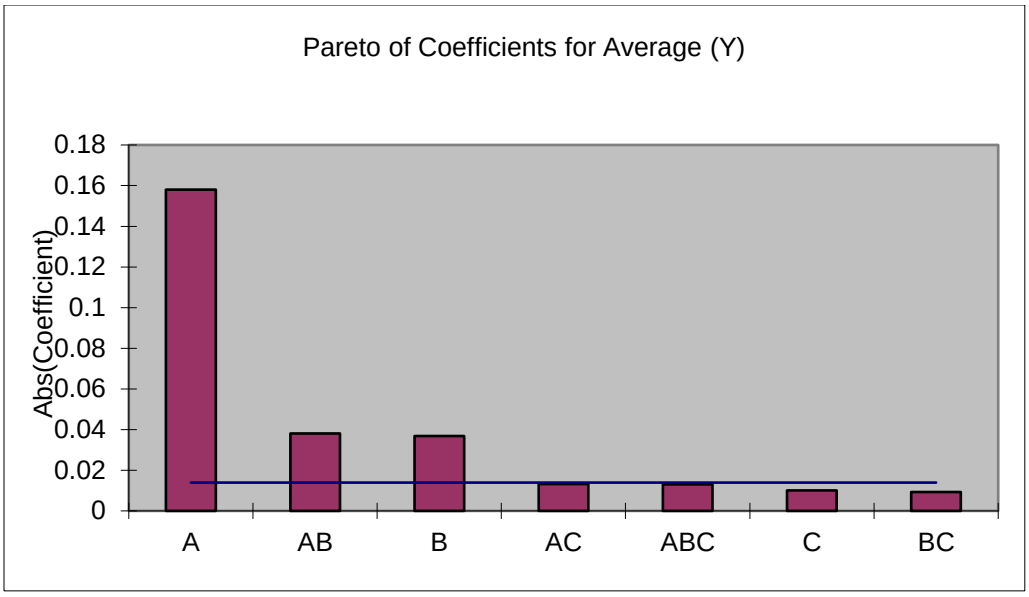

Figure 20: Effects of parameters for Slow Separation test. Bar graphs represent relative effect on testing output. Horizontal blue line signifies cut off limit for statistical significance

4.3 Summary

It's important to remember that the results from these tests are specific to the design space of 1-10N of force, a contact area between 225-2500mm^2 and a separation distance from 1-35mm for a material pair of Teflon tape and cardstock as a triboelectric material set (Figure 21) . While the data presented here is specific to this design space, it could offer insight to trends that could be seen in different material sets or expanded design spaces.

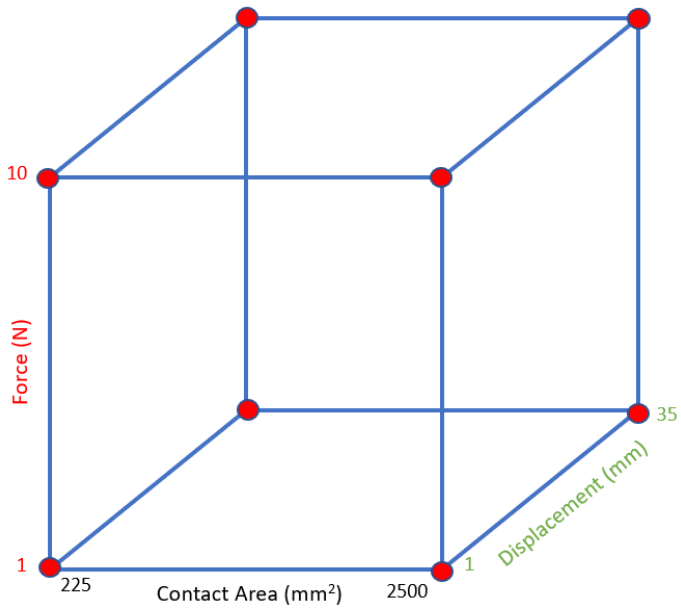

Figure 21: Experimental triboelectric design space. Results of data provide a predictive value within these bounds.

In Table 11, the maximum voltage outputs for each test setup have been boldened. As was discussed in the various sections, for the contact step of actuation the configurations with the smallest contact area and highest force produced the most voltage. This is attributed to the amount of pressure being applied to the samples as they come into contact. For configuration C of the Fast Contact dataset, the approximate amount of pressure applied to the contact pads was 44kPa. In the case of the separation step, the configurations with the largest contact area and force produced the highest voltages.

During the contact step, a fast contact speed produced a higher voltage, whereas the opposite is true for the separation stage. Having a slower separation rate produces the most voltage output. Additionally, in both fast and slow contact/separation, the amount of displacement between 1mm and 35mm only marginally affected voltage output on the order of roughly ~10mV difference in most cases. This is more noticeable when comparing the effects and interactions overview.

Table 11: Summary of test setup output voltages

				Average Voltage			
Configuration	Area (mm^2)	Force (N)	Displacement (mm)	Fast Contact	Slow Contact	Fast Separation	Slow Separation
A	225	1	1	0.629	0.3351	0.0307	0.0224
B	2500	1	1	0.265	0.1511	0.1373	0.3144
C	225	10	1	**1.083**	**0.7662**	0.0274	0.0273
D	2500	10	1	0.526	0.3694	**0.2683**	**0.4197**
E	225	1	35	0.645	0.3424	0.0362	0.0361
F	2500	1	35	0.276	0.1539	0.1375	0.2236
G	225	10	35	**1.215**	**0.7512**	0.0367	0.0261
H	2500	10	35	0.594	0.3714	**0.3029**	**0.4180**

The summary of the effects and coefficients of the testing data in Table 12 shows the significant coefficients in bold, while coefficients in black font denotes insignificance. There is a noticeable trend where different effects and interactions drop below the level of significance when the testing is done with a slower contact or separation speed.

For the contact step coefficients, the negative value for contact area (E_1) in both fast and slow tests implies that while it is significant, it will negatively impact the voltage output. Conversely, the separation step coefficients point to increasing the contact area to increase voltage output.

In both cases where an effect/interaction drops below the significance threshold, it was always the displacement distance, or an interaction shared with it. In all testing data, the displacement between the two materials pads seemed to provide the smallest amount of influence to the voltage output. This can be seen in the low values of all the displacement interaction coefficients

in Table 12 (I_{13}, $I_{23,}$ I_{123}). The takeaway from this is how little the displacement distance influences voltage output for this design space.

Table 12: Summary of coefficients of main/interaction effects

Effect/ Interaction	Fast Contact	Slow Contact	Fast Separation	Slow Separation
E_1 (C. Area)	-0.478	-0.287	0.178	0.316
E_2 (Force)	0.400	0.318	0.073	.0736
E_3 (Displacement)	0.056	-7E-04	0.012	-0.02
I_{12}	-0.111	-0.101	0.074	0.076
I_{13}	-0.017	0.003	0.005	-0.026
I_{23}	0.043	-0.005	0.009	0.018
I_{123}	-0.014	0.005	0.007	0.026

Table 13: Regression equations from Design of Experiments

Definition of Parameters	Experimental Mode	Regression Equation
E_1-Contact Area E_2-Contact Force E_3- Separation Distance	Fast Contact Slow Contact Fast Separation Slow Separation	$Y = 0.65 - 0.24E_1 + 0.2E_2 - 0.03E_3 - 0.06I_{12} - 0.009I_{13} + 0.022I_{23} - 0.007I_{123}$ $Y = 0.41 - 0.14E_1 + 0.16E_2 - 0.05I_{12}$ $Y = 0.12 - 0.09E_1 + 0.037E_2 + 0.006E_3 + 0.04I_{12} + 0.003I_{13} + 0.005I_{23} + 0.004I_{123}$ $Y = 0.19 - 0.16E_1 + 0.04E_2 - 0.04I_{12}$

From this design of experiments within this given design space, several key take aways can be found:

- The **displacement distance** of the material pair in contact-separation mode has **little to no impact on voltage output**.
- For the **contact step** portion of the design, a **smaller contact area and high force will produce a higher voltage** as the output appears to be tied to pressure as the driving factor. (Figure 22 A)
- For the **separation step** portion of the design, **increasing the contact area will produce more voltage** in addition to the force applied. (Figure 22 B)
- While not examined, **impulse may be a variable** of consideration to the difference in output between the fast and slow contact steps.

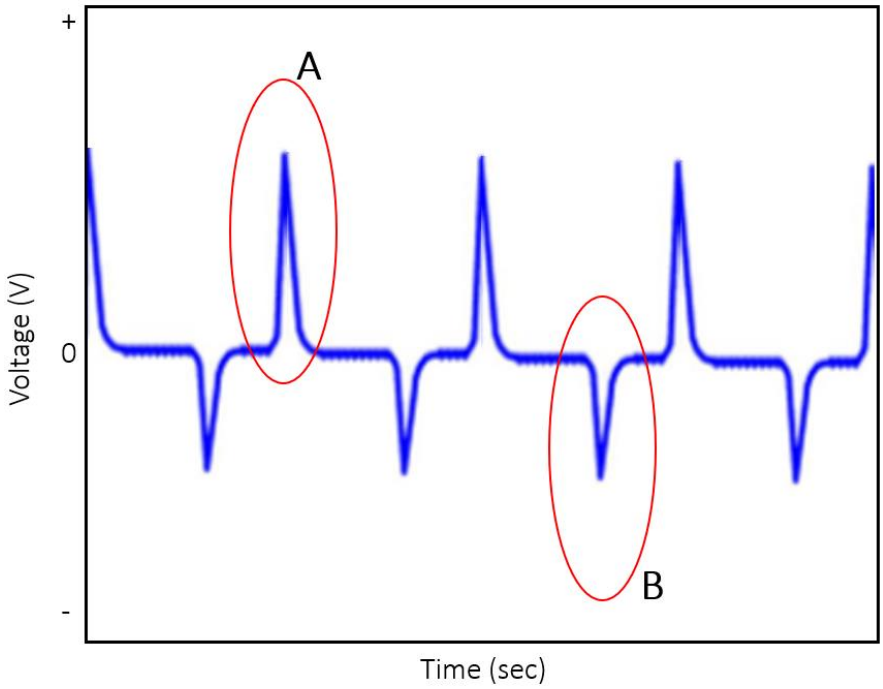

*Figure 22: Arbitrary triboelectric output waveform. **A** represents the output during the contact step, **B** the separation step.*

5. Conclusions and Recommendations

The focus of this thesis' experimental plan was to perform an analysis of 3 parameters of a triboelectric device: contact area, contact force, and displacement distance. Using a Design of Experiments approach, each individual main effect and interaction could be measured to determine which of the parameters influenced the voltage output the most.

Early into testing, during the shakedown process wherein issues in the testing setup are found, it became obvious that there were other factors that were not accounted for in the initial tests. This moved the experimental method down a path of testing both the contact portion of the system and the separation portion of the system and seeing how the chosen parameters changed depending on the portion of contact separation examined.

The results of the Design of Experiments showed that depending on the stage of contact separation that is analyzed, the main effects and interactions changed. For the contact stage, a smaller contact area with a higher force would produce a greater voltage output. The main effect of contact area actually has a negative coefficient in the regression equation meaning that as the contact area is increased, it will reduce the voltage output. During the separation stage, the opposite is true, having a larger contact area improved voltage output in addition to the force applied. Finally, in both contact and separation stages, the displacement distance showed no notable effect on voltage output.

These concluding results are specific to this design space and this material set; however they can provide insight into design consideration of a triboelectric device and how it is designed IE designing a device that is meant to focus primarily on the separation step of the contact separation cycle based on where the device is intended to be installed/ used.

These results are interesting as compared to Vasandani et al. in their paper covered in the literature review section. Vasandani et al. concluded that the main effect their simulation and experimental tests showed that separation distance was the main effect contributing to voltage output, however the material set they tested differed from the ones chosen for this thesis.

To expand outside the work of this thesis, it would be interesting to see if the parameters that were used to test voltage output were used to test current output. The results could show an optimal setup for a triboelectric device designed to power a high current load rather than a high voltage load. Lastly, a deeper look at how the impulse during the contact step influences output could better explain the correlation between contact area, force and pressure to output voltage.

6. References

[1] Z. L. Wang, L. Lin, J. Chen, S. Niu, and Y. Zi, *Triboelectric Nanogenerators*. Cham: Springer International Publishing, 2016. doi: 10.1007/978-3-319-40039-6.

[2] C. Zhang *et al.*, "Harvesting Wind Energy by a Triboelectric Nanogenerator for an Intelligent High-Speed Train System," *ACS Energy Lett.*, pp. 1490–1499, Mar. 2021, doi: 10.1021/acsenergylett.1c00368.

[3] S.-F. Leung *et al.*, "Blue energy fuels: converting ocean wave energy to carbon-based liquid fuels *via* CO_2 reduction," *Energy Environ. Sci.*, vol. 13, no. 5, pp. 1300–1308, 2020, doi: 10.1039/C9EE03566D.

[4] Z. Ren *et al.*, "Energy Harvesting from Breeze Wind (0.7–6 m s^{-1}) Using Ultra-Stretchable Triboelectric Nanogenerator," *Adv. Energy Mater.*, vol. 10, no. 36, p. 2001770, Sep. 2020, doi: 10.1002/aenm.202001770.

[5] Y. Yang *et al.*, "Pyroelectric Nanogenerators for Harvesting Thermoelectric Energy," *Nano Lett.*, vol. 12, no. 6, pp. 2833–2838, Jun. 2012, doi: 10.1021/nl3003039.

[6] Y. Zou, A. Libanori, J. Xu, A. Nashalian, and J. Chen, "Triboelectric Nanogenerator Enabled Smart Shoes for Wearable Electricity Generation," *Research*, vol. 2020, p. 2020/7158953, Jan. 2020, doi: 10.34133/2020/7158953.

[7] G. Zhu, P. Bai, J. Chen, and Z. Lin Wang, "Power-generating shoe insole based on triboelectric nanogenerators for self-powered consumer electronics," *Nano Energy*, vol. 2, no. 5, pp. 688–692, Sep. 2013, doi: 10.1016/j.nanoen.2013.08.002.

[8] H. Ryu, H. Yoon, and S. Kim, "Hybrid Energy Harvesters: Toward Sustainable Energy Harvesting," *Adv. Mater.*, vol. 31, no. 34, p. 1802898, Aug. 2019, doi: 10.1002/adma.201802898.

[9] Q. Wang, M. Chen, W. Li, Z. Li, Y. Chen, and Y. Zhai, "Size effect on the output of a miniaturized triboelectric nanogenerator based on superimposed electrode layers," *Nano Energy*, vol. 41, pp. 128–138, Nov. 2017, doi: 10.1016/j.nanoen.2017.09.030.

[10] D. W. Kim, J. H. Lee, J. K. Kim, and U. Jeong, "Material aspects of triboelectric energy generation and sensors," *NPG Asia Mater.*, vol. 12, no. 1, p. 6, Dec. 2020, doi: 10.1038/s41427-019-0176-0.

[11] Y. Wang, X. Jin, W. Wang, J. Niu, Z. Zhu, and T. Lin, "Efficient Triboelectric Nanogenerator (TENG) Output Management for Improving Charge Density and Reducing Charge Loss," *ACS Appl. Electron. Mater.*, vol. 3, no. 2, pp. 532–549, Feb. 2021, doi: 10.1021/acsaelm.0c00890.

[12] X. He, H. Guo, X. Yue, J. Gao, Y. Xi, and C. Hu, "Improving energy conversion efficiency for triboelectric nanogenerator with capacitor structure by maximizing surface charge density," *Nanoscale*, vol. 7, no. 5, pp. 1896–1903, 2015, doi: 10.1039/C4NR05512H.

[13] L. Lin, Y. Xie, S. Niu, S. Wang, P.-K. Yang, and Z. L. Wang, "Robust Triboelectric Nanogenerator Based on Rolling Electrification and Electrostatic Induction at an Instantaneous Energy Conversion Efficiency of ~55%," *ACS Nano*, vol. 9, no. 1, pp. 922–930, Jan. 2015, doi: 10.1021/nn506673x.

[14] Q. Zeng, A. Chen, X. Zhang, Y. Luo, L. Tan, and X. Wang, "A Dual-Functional Triboelectric Nanogenerator Based on the Comprehensive Integration and Synergetic Utilization of Triboelectrification, Electrostatic Induction, and Electrostatic Discharge to Achieve Alternating Current/Direct Current Convertible Outputs," *Adv. Mater.*, p. 2208139, Dec. 2022, doi: 10.1002/adma.202208139.

[15] C. A. Mizzi, A. Y. W. Lin, and L. D. Marks, "Does Flexoelectricity Drive Triboelectricity?," *Phys. Rev. Lett.*, vol. 123, no. 11, p. 116103, Sep. 2019, doi: 10.1103/PhysRevLett.123.116103.

[16] "Tube-like objects on back of wing [Static Wicks, Static Dischargers]," *Metabunk*. https://www.metabunk.org/threads/tube-like-objects-on-back-of-wing-static-wicks-static-dischargers.6674/ (accessed Jan. 21, 2023).

[17] H. Zou *et al.*, "Quantifying the triboelectric series," *Nat. Commun.*, vol. 10, no. 1, p. 1427, Mar. 2019, doi: 10.1038/s41467-019-09461-x.

[18] R. Zhang and H. Olin, "Material choices for triboelectric nanogenerators: A critical review," *EcoMat*, vol. 2, no. 4, Dec. 2020, doi: 10.1002/eom2.12062.

[19] Z. Zhao *et al.*, "Selection rules of triboelectric materials for direct-current triboelectric nanogenerator," *Nat. Commun.*, vol. 12, no. 1, p. 4686, Aug. 2021, doi: 10.1038/s41467-021-25046-z.
[20] Y. J. Kim, J. Lee, S. Park, C. Park, C. Park, and H.-J. Choi, "Effect of the relative permittivity of oxides on the performance of triboelectric nanogenerators," *RSC Adv*, vol. 7, no. 78, pp. 49368–49373, 2017, doi: 10.1039/C7RA07274K.
[21] L. Dhakar, "Study of Effect of Topography on Triboelectric Nanogenerator Performance Using Patterned Arrays," in *Triboelectric Devices for Power Generation and Self-Powered Sensing Applications*, Singapore: Springer Singapore, 2017, pp. 39–66. doi: 10.1007/978-981-10-3815-0_3.
[22] S. P. Rajeev, S. Sabarinath, C. Subash, U. Valiyaneerilakkal, P. Parameswaran, and S. Varghese, "α- & β-crystalline phases in polyvinylidene fluoride as tribo-piezo active layer for nanoenergy harvester," *High Perform. Polym.*, vol. 31, no. 7, pp. 785–799, Sep. 2019, doi: 10.1177/0954008318796141.
[23] X. Xia, J. Fu, and Y. Zi, "A universal standardized method for output capability assessment of nanogenerators," *Nat. Commun.*, vol. 10, no. 1, p. 4428, Sep. 2019, doi: 10.1038/s41467-019-12465-2.
[24] J. Shao, M. Willatzen, and Z. L. Wang, "Theoretical modeling of triboelectric nanogenerators (TENGs)," *J. Appl. Phys.*, vol. 128, no. 11, p. 111101, Sep. 2020, doi: 10.1063/5.0020961.
[25] N. US Department of Commerce, "How Powerful Is Lightning?" https://www.weather.gov/safety/lightning-power (accessed Jan. 19, 2023).
[26] G. Zhu *et al.*, "Triboelectric-Generator-Driven Pulse Electrodeposition for Micropatterning," *Nano Lett.*, vol. 12, no. 9, pp. 4960–4965, Sep. 2012, doi: 10.1021/nl302560k.
[27] C. Wu, A. C. Wang, W. Ding, H. Guo, and Z. L. Wang, "Triboelectric Nanogenerator: A Foundation of the Energy for the New Era," *Adv. Energy Mater.*, vol. 9, no. 1, p. 1802906, Jan. 2019, doi: 10.1002/aenm.201802906.
[28] S. Wang, L. Lin, Y. Xie, Q. Jing, S. Niu, and Z. L. Wang, "Sliding-Triboelectric Nanogenerators Based on In-Plane Charge-Separation Mechanism," *Nano Lett.*, vol. 13, no. 5, pp. 2226–2233, May 2013, doi: 10.1021/nl400738p.
[29] P. Vasandani, Z.-H. Mao, W. Jia, and M. Sun, "Design of simulation experiments to predict triboelectric generator output using structural parameters," *Simul. Model. Pract. Theory*, vol. 68, pp. 95–107, Nov. 2016, doi: 10.1016/j.simpat.2016.08.002.